



# Microstructure and Mechanical Characterization of Al–SiC MMC Tube Produced via Friction Stir Back Extrusion

Masoud Mahmoodi<sup>1</sup>  · Kamin Tahmasbi<sup>1</sup> · Milad Zaroodi<sup>1</sup>

Received: 23 December 2020 / Accepted: 4 June 2021 / Published online: 6 July 2021  
© The Indian Institute of Metals - IIM 2021

**Abstract** Friction stir back extrusion (FSBE) is a new-fangled method to produce high strength tubes with a fine-grained structure. In the following experiment, using a solid cylindrical AA7075 aluminum alloy bar and some SiC powder, the Al–SiC composite tube has been produced by the process of FSBE. To examine the microstructural properties of samples, both the scanning electron microscopy and optical microscopy were applied. Microhardness and tensile tests were also used to assure mechanical properties of the tubes. Furthermore, the phase analysis of samples was carried out via the X-ray diffraction technique. It was observed that SiC particles were almost distributed homogeneously among the aluminum phase. In addition, grains sizes of the composite tube were decreased in comparison with the aluminum tube. The XRD pattern analysis of the composite specimen demonstrated that the peaks of Al and SiC appear as the main phase and then new phases of  $Al_4C_3$  and  $Al_4SiC_4$  will emerge subsequent to the process.

**Keywords** Friction stir back extrusion · Tube · Aluminum matrix composite · Silicon carbide · Microstructure

## 1 Introduction

The application of metal matrix composites (MMC) is increasingly scaling up, due to the high strength as compared with the low weight. As a considerable interest, the aluminum–silicon carbide (Al/SiC) composite has appealing properties besides the low cost. SiC has a high hardness, low density, perfect anti-corrosive quality, good wear resistance, scant coefficient of thermal expansion, high thermal conductivity, and is widely used in construction and machinery industries [1, 2]. It's rumored that the aluminum alloy is a proper material in automobile industries, due to their low density, excellent ductility, and outstanding machinability [3, 4]. In Al/SiC composites, Al works as the matrix material and SiC particles play the role of reinforcement phase, in which several superiorities of these two materials, such as low density, easy production, and high specific stiffness are merged [5, 6].

The Al/SiC composite can be made using different techniques such as stir casting and powder metallurgy. However, inhomogeneous distribution of SiC in the matrix and wetting intricacies of SiC and Al matrix are included as some of its significant problems [7]. There is a need to develop new processing approaches to solve the above problems. Friction stir extrusion (FSE) is a method of recycling that was firstly established by Thomas et al. [8]. Due to the friction between the die and materials, a large amount of heat is released in this method. The softened and consolidated metal will be extruded out and under the high pressure, finally forms a wire. The production of AA2195 and AA2050 aluminum wires through the FSE method has been studied by Tang and Reynolds [9]. They showed that this volume of released heat, which depends on the rotational speed, is considered as an effective factor in the quality of fabricated wires. Sharifzadeh et al. [10] extruded

✉ Masoud Mahmoodi  
mahmoodi@semnan.ac.ir

<sup>1</sup> Faculty of Mechanical Engineering, Semnan University,  
3513119111 Semnan, Iran

magnesium wires via FSE method and probed the wear and corrosion resistance of wires. The heat transfer phenomenon and also temperature field during the friction extrusion process were simulated by Zhang et al. [11]. They measured temperature variations experimentally. Using XRD profile analysis and Rietveld method, Tahmasbi and Mahmoodi [12, 13] experimentally recycled AA7022 wire via FSE method and evaluated microstructural and mechanical properties of wires. Furthermore, the result of corrosion tests show that the samples have adequate corrosion resistance. In addition, the acceleration of die rotation rate enhances the density and subsequently reduces the corrosion resistance.

To fabricate tubes with fine-grained microstructure, the novel process of friction stir back extrusion (FSBE) was developed by Abu-Farha [14]. He studied the microstructure of AA6063-T52 aluminum tube from different aspects. As well, Sarkari and Movahedi [15] fabricated the aluminum tube through FSBE process and investigated its mechanical and microstructural properties. Dinaharan et al. [16] also produced the pure copper tube via FSBE method and studied its microstructural characteristics. Using the Shear Assisted Processing and Extrusion (ShAPE) machine, Whalen et al. [17, 18] extruded magnesium alloy tubes of ZK60 and AZ91E. They showed that the produced samples represent appropriate microstructure and crystallographic texture, which increase their ductility and toughness.

Recently, many types of researches have been conducted on the possibility of producing metal matrix composites recurring to the new technologies, such as friction stir-based technologies. Dolatkhan et al. [19] surveyed the effect of process parameters on the fabrication of AA5052/SiC metal matrix composite through friction stir processing (FSP), although the same technologies were implemented to AA2024/SiC [20] and Al/Graphene [21]. Baffari et al. [22] recently began to research the production of Al-SiC metal matrix composite wire through FSE of aluminum chips and examine the microstructure of composite wires. However, most of researches on FSBE method have been carried out on metals without any reinforcement.

The result of experiments on FSBE of AA7075 aluminum alloy billet, aiming at the production of MMC tube by adding SiC powder to the billet, is presented in this paper. Microstructural and mechanical properties of the MMC tube as compared to the aluminum tube properties are investigated here.

## 2 Experimental Procedures

### 2.1 Materials

To fabricate the composite tube, an AA7075-T6 aluminum cylindrical billet with a diameter of 19 mm and the length of 35 mm was used as a matrix material, and SiC powders were acting as reinforcement factors. The nominal composition of AA7075-T6 aluminum alloy is shown in Table 1. This kind of alloy has a high strength and toughness; so has an extensive application in automotive industries. The average size of SiC particles used in the present study is about 4  $\mu\text{m}$ . Furthermore, the density of AA7075-T6 aluminum alloy and SiC powder is, respectively, about 2.77 and 3.21  $\text{gr}/\text{cm}^3$ . It is noteworthy to mention that eighteen holes with an average diameter of 1.5 mm were created along the cylinder to embed SiC powders inside the aluminum billet. The aluminum billet stuffed with SiC powders pressed into the holes which are shown in Fig. 1. According to the dimensions and density values of materials indicated in Fig. 1, both the volumetric percentage and weight percentage of the composite have been calculated that their formulas are as the following. Letters of  $V$ ,  $m$  and  $\rho$ , respectively, stand for the volume, mass and density of the materials.

$$V_{(\text{SiC})} = \text{Total No of holes} \times \text{Volume of one hole} = 18 \times \pi \times (0.075^2) \times 3 = 0.95 \text{ cm}^3$$

$$m_{(\text{SiC})} = \rho_{(\text{SiC})} \times V_{(\text{SiC})} = 3.04 \text{ gr}$$

$$V_{(\text{BM})} = \text{Volume of processed base material} = (\pi \times (0.95^2) \times 3.5) = 9.92 \text{ cm}^3$$

$$m_{(\text{BM})} = \rho_{(\text{BM})} \times V_{(\text{BM})} = 27.47 \text{ gr}$$

$$\text{Volume \% of SiC} = \frac{V_{(\text{SiC})}}{V_{(\text{BM})}}$$

$$= 9.58\% \quad \text{Weight \% of SiC} = \frac{m_{(\text{SiC})}}{m_{(\text{BM})}}$$

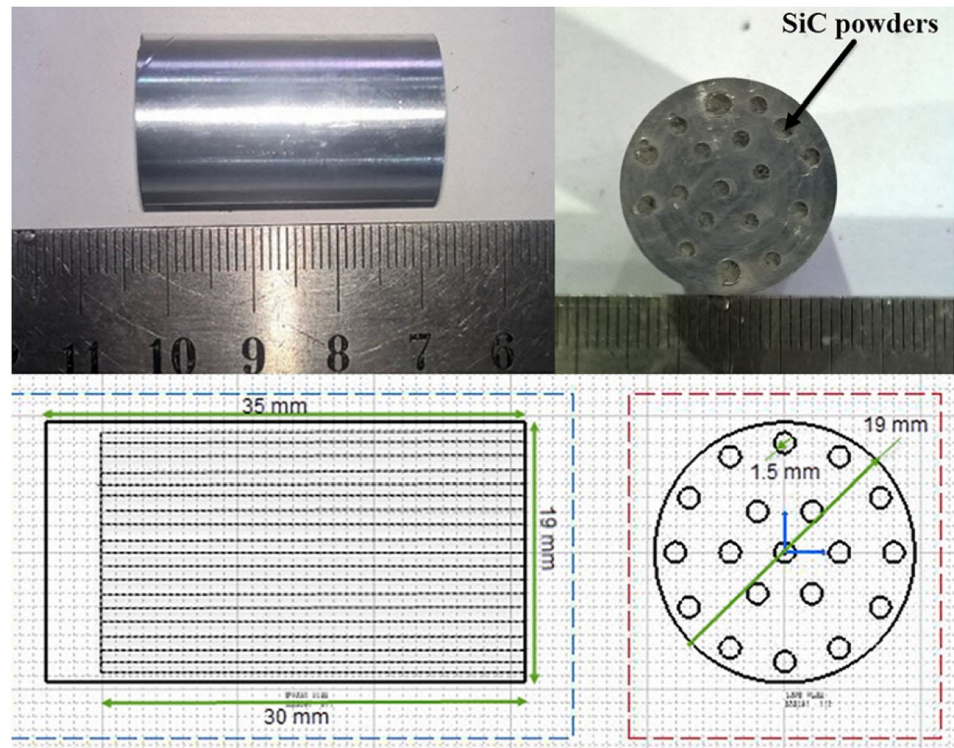
$$= 11.07\%$$

### 2.2 Friction Stir Back Extrusion

In the current experiment, the AA7075 aluminum matrix composite reinforced by SiC particles was fabricated by FSBE method using a modified lathe and combined with a self-made fixture. The composite tube's fabricating procedure is displayed in Fig. 2. The FSBE setup used in this work consists of two main components, namely the plunging tool and rotary billet chamber. In this setup, the plunging tool was plunged into a cylindrical billet constrained in the rotary billet chamber. The heat generated by the friction of the tool and billet was sufficient to soften the material and made it easy to deform. The integration of axial and rotational motions in the plunging tool and rotary billet chamber simply enforced the material to extrude outwards. The stirring action under a relatively high

**Table 1** Chemical composition of 7075-T6 aluminum alloy

Elements	Al	Zn	Mg	Cu	Fe	Mn	Si	Cr	Ti
Wt%	Bal	5.1	2.1	1.2	< 0.5	< 0.3	< 0.4	0.18	< 0.2

**Fig. 1** The AA7075 aluminum cylinder billet with SiC powders pressed into the holes

pressure imposed a severe plastic deformation on the material and thus refined its grain structure.

A plunging tool was made of H13 tool steel designed with a diameter of 13 mm. The furthest back of plunging tool was tapered to an angle of  $10^\circ$  to make the extrusion process easier. The taper angle can be considered the same as the extrusion angle in a conventional extrusion. The rotary billet chamber was designed in a cylindrical shape, split into two halves to facilitate the specimen extraction after testing. The rotary billet chamber was also made of H13 tool steel and was tempered. The height of rotary billet chamber was 80 mm, and a hole of 19 mm to a depth of 65 mm was worked out in the center. It is noteworthy to say that the extrusion ratio was 1.88 ( $A_1/A_2$ ), in which  $A_1$  is the initial billet's cross-sectional area and  $A_2$  is the final tube's cross-sectional area. The special fixtures were made of mild steel to hold the components in a steady state during FSBE process. Both the experimental setup and fabricated die are illustrated in Fig. 3.

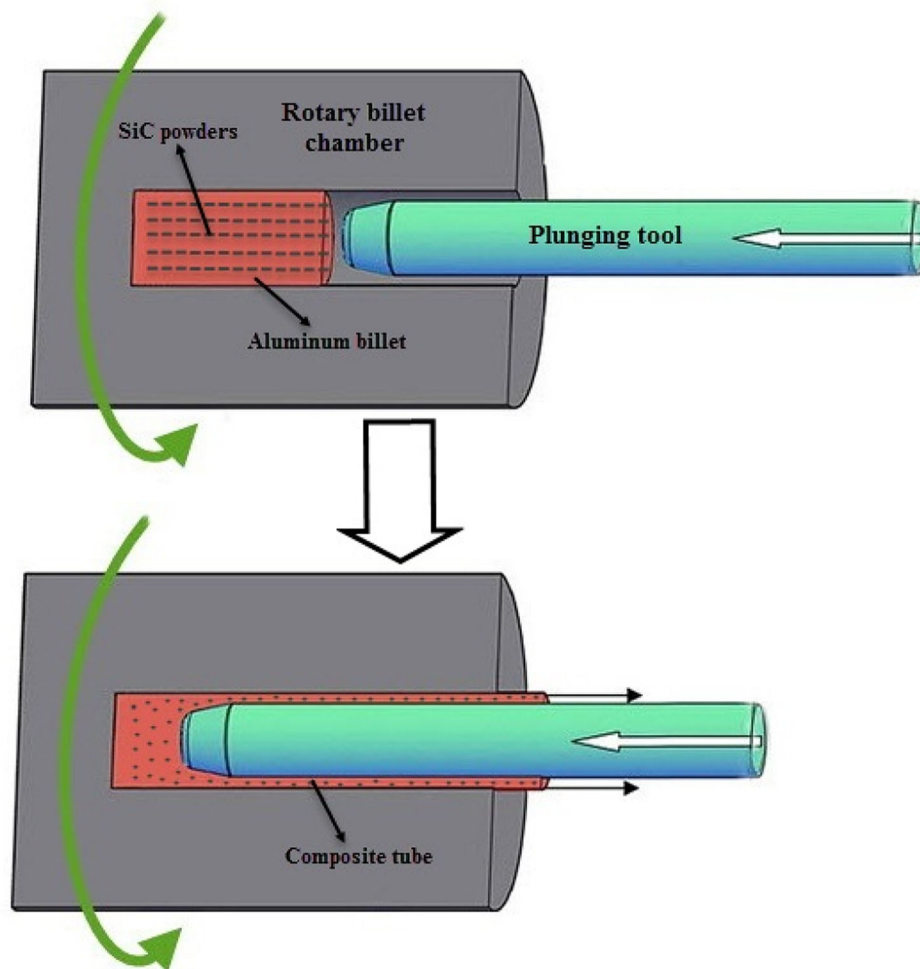
The rotary billet chamber was rotated at 1400 rpm, and the plunging tool was driven into the billet with an axial

feed rate of 1.2 mm/s and an axial force of 15.38 KN. Both the extrusion force and the axial feed rate were measured and controlled by the hydraulic system's pressure control and flow control valves. To study the effect of SiC particles, a non-composite AA7075 aluminum tube without SiC powders was also fabricated at the same condition.

### 2.3 Microstructure Characterization and Mechanical Testing

To observe and test, the processed samples were scarped perpendicular to the FSBE direction by the electron discharge machining. Then, the specimens were carefully ground, polished, and etched according to the standards of ASTM E407-07 and ASTM E3-11. The microstructure of samples was observed by OLYMPUS BH2-UMA optical microscopy (OM) and JEOL JXA-840 scanning electron microscopy (SEM), and the average grain size of samples was calculated by the mean linear intercept method. Microhardness tests were performed at the transverse cross section of the samples using a Vickers digital

**Fig. 2** Schematic of FSBE process to produce composite tube



microhardness tester (MMT-7/Buehler) under a load of 50 g for 10 s. In this test, the hardness of tubes was measured from the interior cortex to the exterior cortex with intervals of 0.25 mm. To ensure the precision of test findings, samples were tested three times, and the average values were regarded as experiment results. The tensile test was also conducted in order to evaluate the tubes' mechanical properties. The feed rate of tensile test machine's jaw was 0.1 mm/min. According to ASTM E8-M, two samples of tensile test were provided for each tube. The dimensions of test specimens are depicted in Table 2. Moreover, an annealed piece of base material (BM) was investigated to compare the properties of produced tubes with the base material.

#### 2.4 X-Ray Diffraction

The X-ray diffraction test was performed on the tube samples. The experiment was carried out using a Bruker/

D8 device with a voltage of 40 kV and an electric current of 40 mA at the ambient temperature. A  $\text{CuK}\alpha$ -ray with a wavelength of 1.54056 Å was used as an X-ray source in the experiment. Samples were examined at the radiation angles between 10° and 90° and the speed of 0.06°/s. Subsequently, X'Pert High Score software was utilized to obtain and analyze the XRD pattern.

### 3 Results and Discussion

#### 3.1 Samples Quality

AA7075 aluminum tube and Al-SiC composite tube have been fabricated by the FSBE process. The typical image of tubes is depicted in Fig. 4a. The figure shows that tubes' cortices are formed completely and there are no cracks or defects in cross sections. As observed, the tubes' interior and exterior cortices have a relatively rough surface



**Fig. 3** **a** The experimental setup **b** rotary billet chamber **c** plunging tool

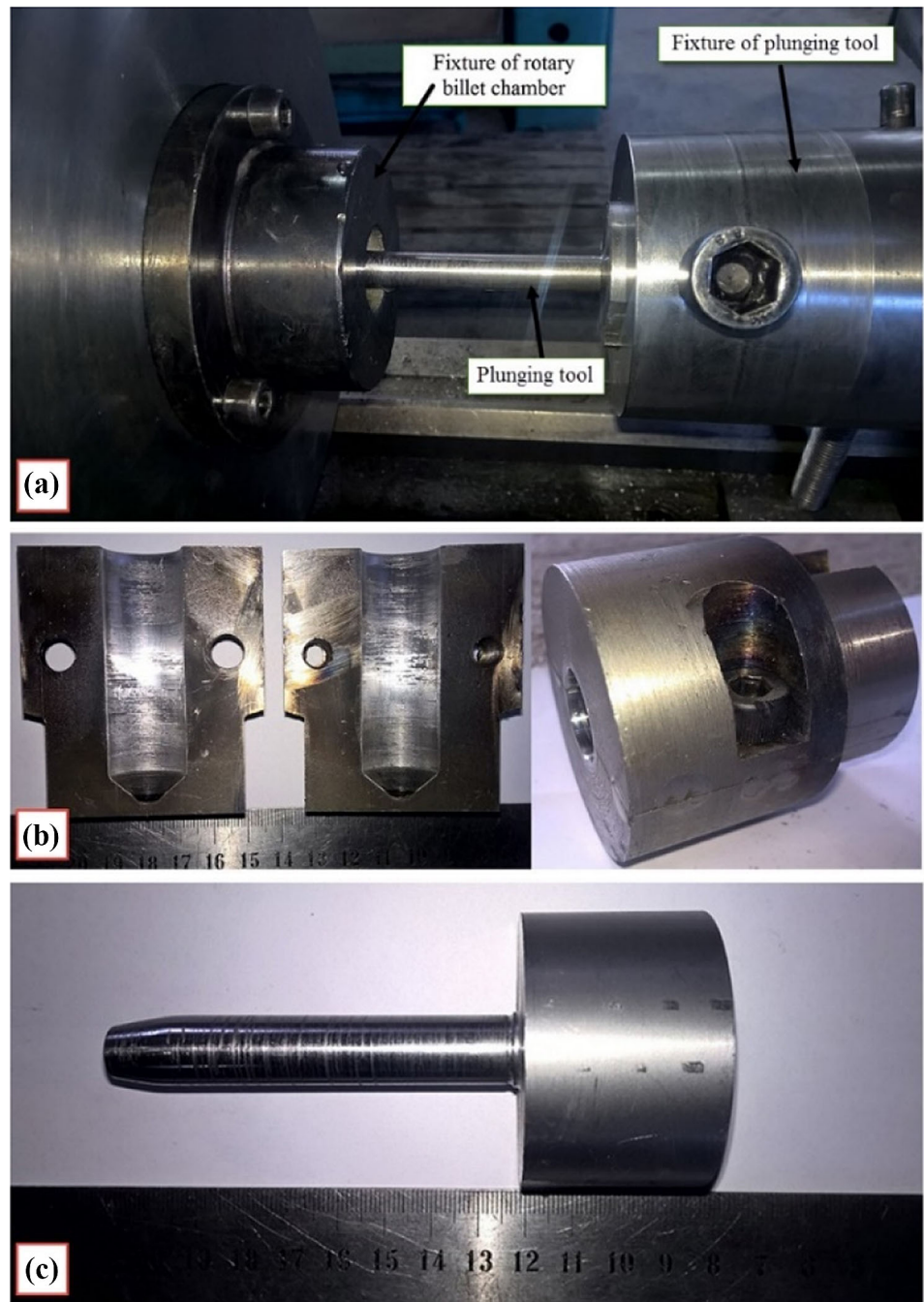


**Table 2** Dimensions of the tensile test specimens

Specimen	The aluminum tube	The composite tube
Width	3.93 mm	4.28 mm
Thickness	2.97 mm	3.09 mm
Cross-sectional area	11.67 mm <sup>2</sup>	13.22 mm <sup>2</sup>
The distance between the jaws after fixing	47 mm	48 mm

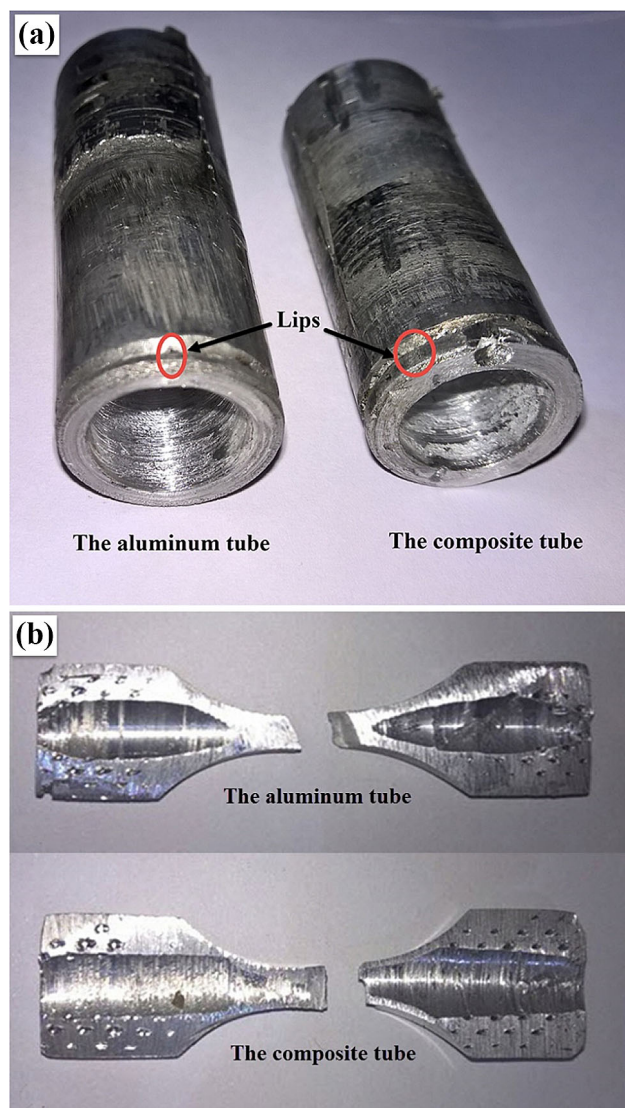


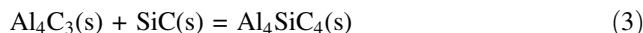
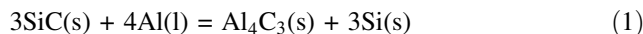
**Fig. 4** a The image of tubes formed by FSBE process b Tensile test specimens of the same tubes

quality; it could be due to the low degree of surface finish (surface texture or surface topography) of the plunging tool and also the rotary billet chamber's hole. So the tubes require further machining operation before actual use. The integration of dies' axial and rotational movements enforce the plasticized material to go through three-dimensional spiral paths; so, the material is twisted during the tubes' formation. A lip is formed at the end of the tubes, but it is negligible in the primary stages of the manufacturing process. As can be seen, the composite tube's lip is formed non-homogeneously since the holes of initial billet are filled with SiC powder. Figure 4b also demonstrates the same samples which are fractured after the tensile test. Curved and flattened spots caused by the tensile machine grip could be observed in the figure too.

### 3.2 X-ray Diffraction Analysis

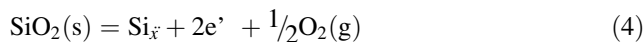
Figure 5 shows XRD patterns of both the aluminum tube and the composite tube fabricated via FSBE method. As inferred from Fig. 5a, only diffraction peaks corresponding to (111), (200), (220), and (311) planes of the aluminum phase with face cubic centered (FCC) structure have been detected. In Fig. 5b, the X-ray diffraction image of composite tube suggests various peaks which represent different phases in the composite sample. The peaks of Al and SiC emerge as the main phases. Aluminum has a low melting temperature which helps to react with SiC powder under the pressure. Theoretically,  $\text{Al}_4\text{C}_3$  will emerge at 400 °C in the Al–C–Si phase diagram and it can be easily detected at 580 °C in the traditional method.

The expected reaction in the Al–C–Si system may be defined as follows:



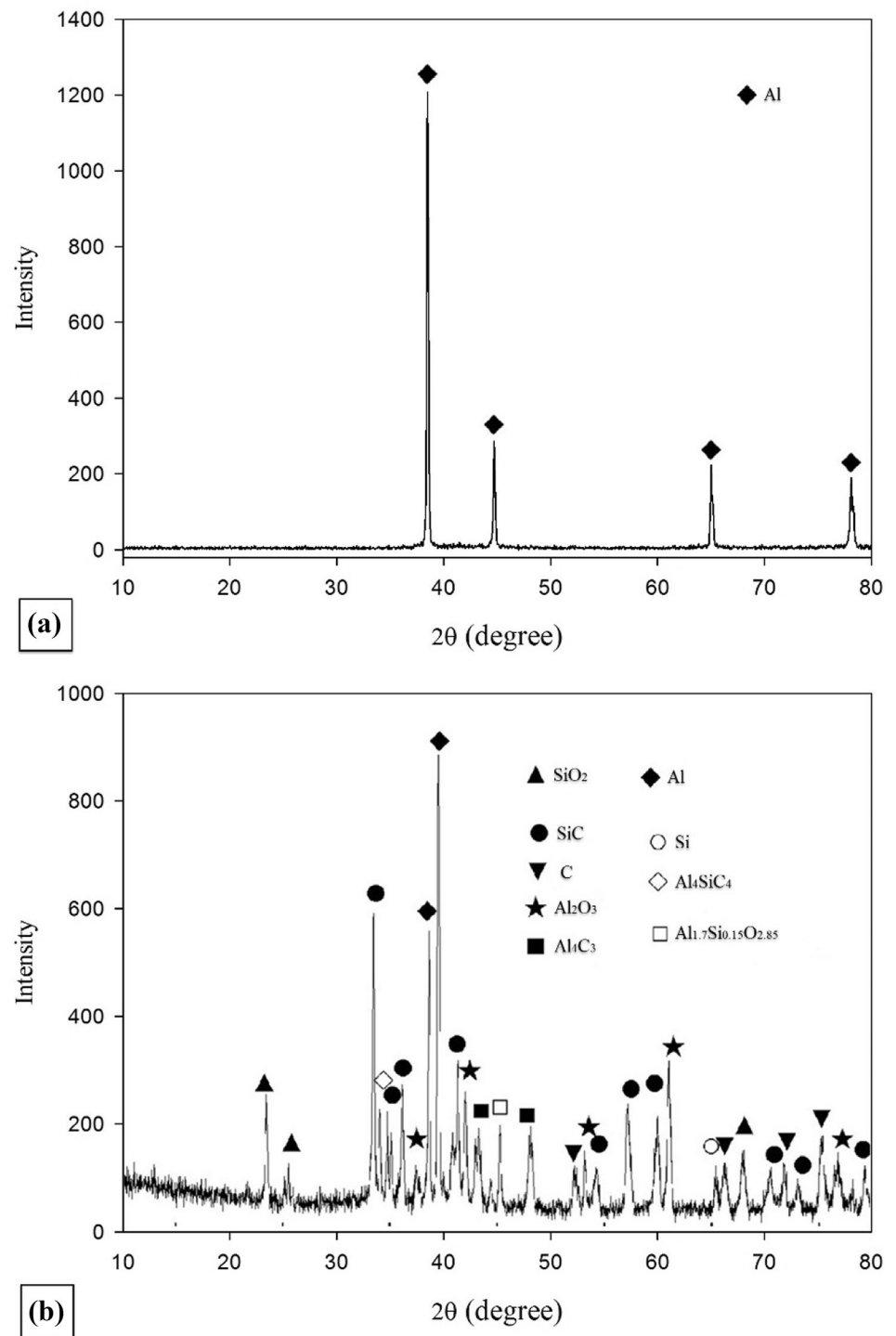
According to Fig. 5b, the peaks of Si and C were obtained from XRD image. By analyzing SEM image of the composite tube, just a little filamentary  $\text{Al}_4\text{C}_3$  could be seen in the composite. The  $\text{Al}_4\text{SiC}_4$  phase is dispersed like a needle confronting with the Al/SiC composite sample. This phase is detected by X-ray and it's indicated in the XRD image. SiC could be easily oxidized into  $\text{SiO}_2$  since a little oxygen is mixed. The  $\text{SiO}_2$  peaks are also detected in the XRD image.

Several peaks of  $\text{Al}_2\text{O}_3$  are detected in the XRD image of the composite tube. Considering that the aluminum is a fairly active metal; hence, some of Al oxidizes into  $\text{Al}_2\text{O}_3$  in the drying stage. During the chemical reaction,  $\text{Al}^{3+}$  ion is replaced by  $\text{Si}^{4+}$ , so it leads to form a nonstoichiometric compound as  $\text{Al}_{2-2x}\text{Si}_x\text{O}_{3-x}$  [23–25]. When a high valence cation is displaced by a low valence cation, an anion vacancy is formed. Simultaneously, the cation enters into the solid solution's gaps. According to the electronic conservation technique,  $\text{Si}^{4+}$  ion which replaces  $\text{Al}^{3+}$  obtains an electron. Contrarily, oxygen ion ( $\text{O}^{2-}$ ) loses an electron and  $\text{O}_2$  is created. The reaction is summarized in the following.



Al and SiC can also be oxidized by the generated oxygen that is a positive reaction. Some  $\text{Al}^{3+}$  are replaced by  $\text{Si}^{4+}$  and part of  $\text{O}^{2-}$  fills the anion vacancy. Thus, according to the above analysis, the nonstoichiometric compound of  $\text{Al}_{1.7}\text{Si}_{0.15}\text{O}_{2.85}$  is formed.

**Fig. 5** X-ray diffraction pattern of **a** the aluminum tube **b** the composite tube



### 3.3 Microstructural Investigations

The microstructures of tubes and the base material are shown in Fig. 6. The average grain sizes of base material, aluminum tube, and composite tube are, respectively,

estimated as 39  $\mu\text{m}$ , 21  $\mu\text{m}$ , and 13  $\mu\text{m}$ . As witnessed, the grain sizes decrease during FSBE process. The die's stirring motion creates severe plastic deformation and frictional heat. Therefore, the dynamic recrystallization occurs and produces a fine-grained structure [26]. The parameters



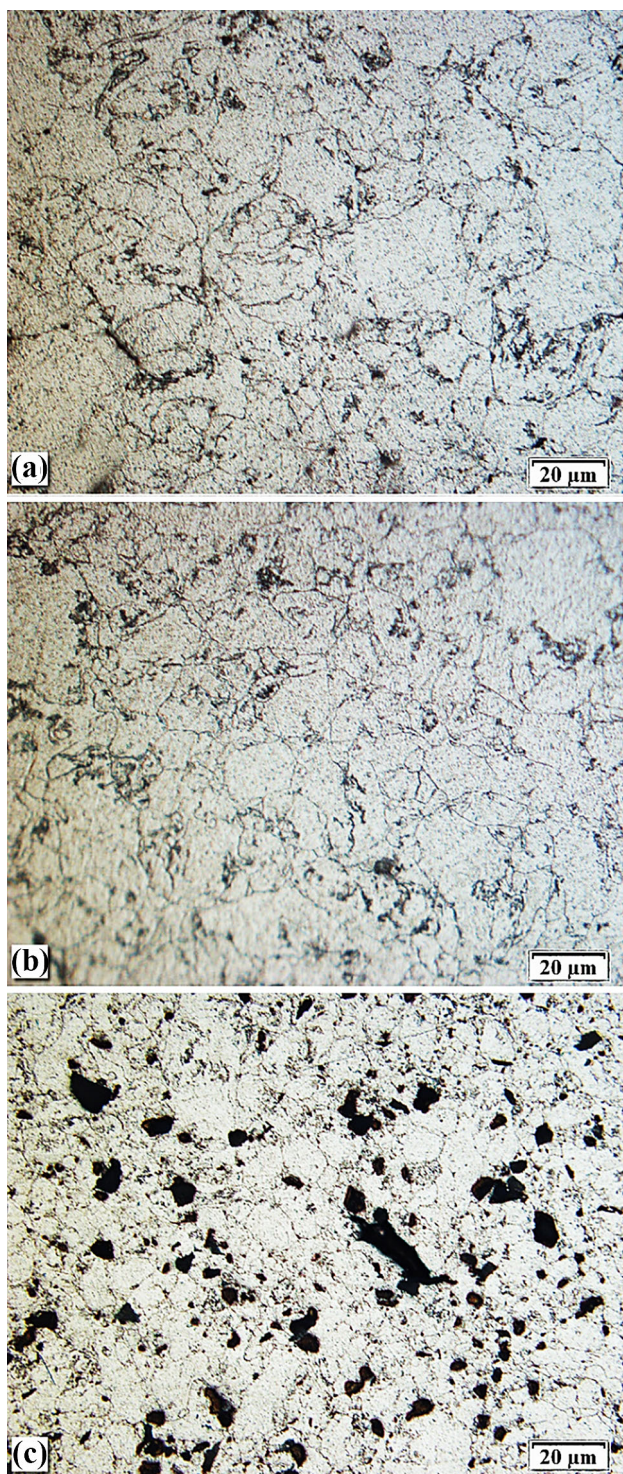


**Fig. 6** Optical micrographs of **a** base material **b** the aluminum tube **c** the composite tube

of FSBE process—including axial feed, plunging tool geometry, rotational speed, and extrusion ratio—can affect the depth of stirring zone and material flow characteristics. The higher the rotational speed, the more heat is input during the FSBE process; so it makes the material flow

easier, nevertheless can lead to the more grain growth and devaluation of the produced tube's mechanical properties. Furthermore, there will be some stickiness between the material and the tool. Lowering the axial feed rate leads to increment of grains sizes and subsidence of the mechanical properties due to the excessive heat input [27].

It is evident from Fig. 6b, c that the composite tube's grain size is lower than the aluminum tube's. The silicon carbide particles in the composite tube structure acts as an obstacle to the grain growth and reduces the grain size; this is called Pinning. But it is possible that with increment of

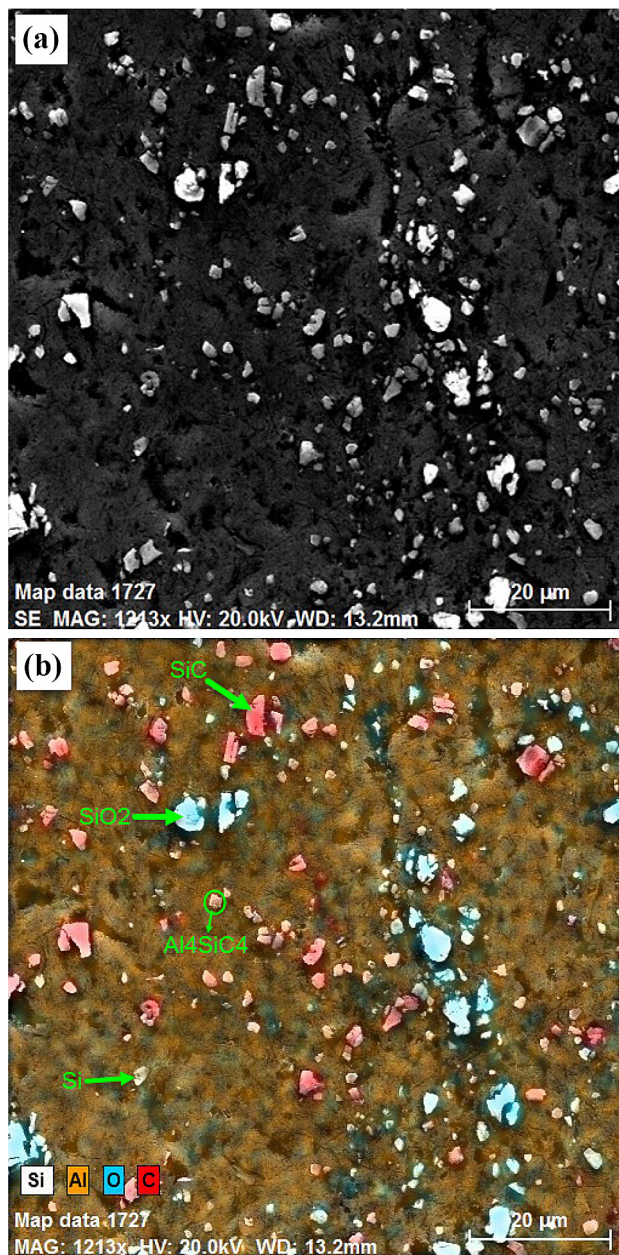


**Fig. 7** **a** SEM image of the composite tube **b** EDX image of the composite tube



temperature during the process, the energy volume stored in grain boundary will rise and cause the grain growth. During recrystallization, on the other hand, silicon carbide particles will act as a context for homogeneous germination and reduce the grain size in the material structure.

The image of composite tube's transverse cross section, taken via SEM, is depicted in Fig. 7. According to Fig. 7a, SiC particles are well distributed in the matrix material. These fragile and hard reinforcing ceramic particles do not deform plastically. So, the densification capacity of the metal matrix composite is affected by enhancing the reinforcement content. The distribution of SiC particles supports a portion of pressure which reduces the transmitted load to the soft plastic particles. The microstructural study implies that the increment of SiC particles quantity enhances porosity rate in the metal matrix composite [28].

The elemental mapping of composite samples with energy-dispersive X-ray (EDX) analysis is shown in Fig. 7b. Different particles created in the aluminum background phase are specified in the figure. Except SiC particles, SiO<sub>2</sub> is noticed in the EDX image as well that could be a protective shell on the SiC surface. In addition, some Al<sub>4</sub>SiC<sub>4</sub> particles are observed in Fig. 7b. The aluminum is well known to have a relatively low melting temperature;

so, it reacts easily with SiC powders under pressure and high temperature of FSBE process.

The EDX analysis of an Al<sub>4</sub>SiC<sub>4</sub> particle is depicted in Fig. 8. The analysis is handled at the range of 4 μm and the period of 37 s. As apparent, the particle length is about 2 μm. According to the line spectrum, the detected particle is SiC; with the beginning of particles variation, in particular the decline of aluminum quantity, the percentage of silicon and carbon elements is scaled up.

### 3.4 Mechanical Properties

Figure 9 illustrates the Vickers microhardness of tubes and base material. The error bars in the figure represent one standard deviation. As obvious, microhardness of the aluminum tube is significantly lower than the composite tube's and microhardness of the base material is lower than both tubes', and the variation of microhardness is smaller. When a proper amount of force is exerted into the plastic flow during FSBE process, the carbide particles disperse between the grain boundaries (Fig. 6c) and the microhardness increases far above the base material state. Also, the samples' microhardness increases by recrystallized fine grains during FSBE process. It should be noted that the material with fine grains is usually harder and stronger than

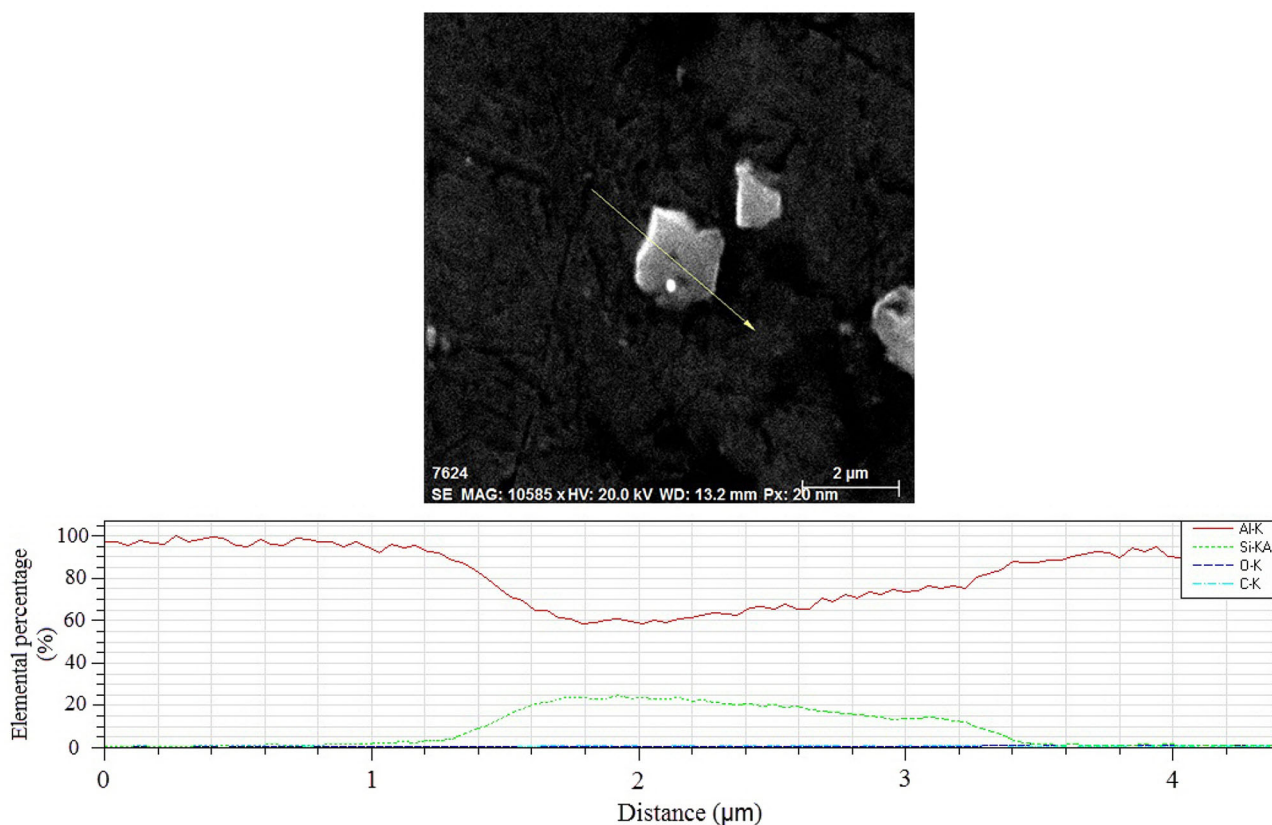


**Fig. 8** EDX analysis of SiC particle

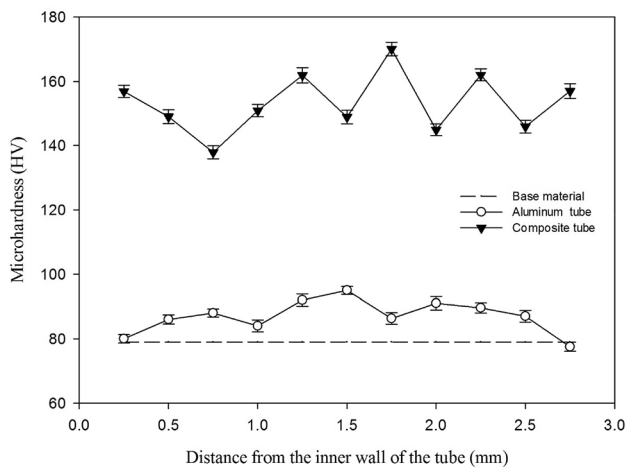


**Fig. 9** Vickers microhardness of both the composite and aluminum tubes produced by friction stir back extrusion

the one with coarse grains, because of the larger total area of grain boundaries in order to limit the dislocations' movement. Accordingly, in the material processing, the smaller the particle size and the more homogeneous the SiC particles' distribution, the higher the tubes' microhardness and the lower the variation of microhardness. Deore et al. [29] have recently carried out a microhardness study on AA7075/SiC composite's component fabricated via friction stir process. For FSP with 5 vol. % SiC filler, they obtain an average hardness of 184 HV. In the present study, an average hardness of 160 HV would be observed, which is lower than Deore's study. It could be owing to less homogenous microstructure resulted from FSBE in comparison with FSP.

The disordered distribution of hardness values could emanate from the SiC particles' inhomogeneous distribution in the AA7075–SiC composite tube. The SiC particles' inhomogeneous distribution in the matrix material could be described as the agglomeration of ceramic particles and it causes part of the material to be harder than another part. Additionally, the AA7075-T6 alloy has been strongly aged naturally and it heavily relies on precipitates (by T6 condition), so it could also be a potential reason for enhancing the hardness after the process. Age-hardening is a consequence of precipitation. The alteration of mechanical properties is due to the precipitate's formation over time. Probably that's why the natural age-hardening happens to samples after the extrusion process in the long term [30].

Elongation to fracture, yield strength, and ultimate tensile strength (UTS) are important parameters to evaluate the mechanical properties. Figure 10 illustrates the samples' tensile testing result. It is remarkable that the strength of both tubes exceed the strength of the base material and the strength of the composite tube is higher than the

aluminum tube's. Regarding the work of Netto et al. [31], in which they manufactured Al7075/NiTi composites via FSP, the mechanical strength is comparable to the result of their study. Although they used different reinforcements and procedures for fabricating Al7075 matrix composites, it can be seen that the range of yield strength and UTS is almost the same. The SiC particles at grain boundaries can change the mechanical behavior of the composite tube. By accumulation of dislocations behind obstacles such as carbide particles and grain boundaries, dislocations' slips are diminished; consequently, the yield strength of material increases.

The FSBE process plastically deforms the matrix and forms high-density dislocations in a part of it, which also elevate the composite's strength [32, 33]. Furthermore, according to the Hall–Petch equation, it is understood that the finer the grain, the more the grain boundaries produced. Hence, dislocations' slips occur hardly, which results in the greater stress needed to deform the material, namely the mechanism of fine-grain strengthening.

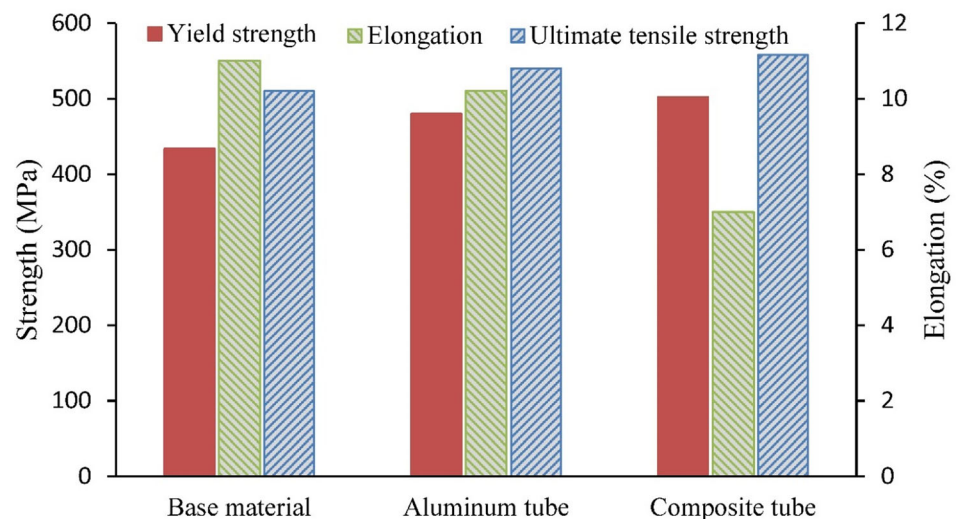
According to Deng and Chawla [34], an increase in particle clustering can result in slightly higher yield strength, while accompanies with a significant reduction in ductility. Furthermore, Song [35] reported that the increment of SiC particles' volumetric fraction subtracts the ductility of SiC/Al composites. As expected, the elongation and ductility of the composite tube is lessened when the strength (UTS) is scaled up, for ceramic particles distributed in the matrix material. It can be inferred that FSBE process can be successfully utilized to produce metal matrix composites with improved mechanical properties. Using the nanoreinforcement powder, the improvement in mechanical properties can be further escalated. Thus, this novel manufacturing approach can be employed as a starting point for future studies.

## 4 Conclusion

In this paper, the AA7075–SiC composite tube was produced by FSBE method. The mechanical properties, as well as the microstructural evaluation of produced tubes, were studied in detail. The following findings can be summarized:

1. It was disclosed that FSBE method has the ability of manufacturing tubular composite without any extrusion defects.
2. The microstructure of FSBE samples mainly consisted of fine recrystallized grains, and the grain size of composite tubes decreased as compared to the aluminum tube and base material.

**Fig. 10** Tensile test results of the initial aluminum bar versus fabricated tubes via the FSBE process



- The SEM images showed that SiC particles in the Al/SiC composite tube were almost distributed homogeneously within the Al matrix material. Moreover, some different particles such as SiO<sub>2</sub> and Al<sub>4</sub>SiC<sub>4</sub> were created in the aluminum background phase.
- For SiC particles had been refined and distributed analogously, the strength and microhardness of composite samples were significantly improved.
- Several peaks were illustrated by XRD analysis that represented different phases in the composite tube. During FSBE process, brittle phase of Al<sub>4</sub>C<sub>3</sub> appeared, and subsequently combining with SiC particles, the Al<sub>4</sub>SiC<sub>4</sub> phase was created.

## References

- Kim D, Lee H G, Park J Y, Park J Y, and Kim W J, *Corros. Sci.* **98** (2015) 304.
- Yang H, Zhou X, Yu J, Wang H, and Huang Z, *Ceram. Int.* **41** (2015) 14692.
- Opalka S M, and Zhu T, *Micropor. Mesopor. Mater.* **222** (2016) 256.
- Li Z, Li C, Gao Z, Liu Y, Liu X, and Guo Q, *Mater. Charact.* **110** (2015) 170.
- Wu Y, Zhang J, Liao H, Li G, and Wu Y, *J. Alloys Compd.* **660** (2016) 141.
- Zhang L, Xu H, Wang Z, Li Q, and Wu J, *J. Alloys Compd.* **678** (2016) 23.
- Tang J, Shen Y, and Li J, *J. Manuf. Process.* **38** (2019) 279.
- Thomas W, Nicholas E, and Jones S, *Friction extrusion metal working*, US. NO Patent 5,262,123 (1993).
- Tang W, and Reynolds A P, *J. Mater. Process. Technol.* **210** (2010) 2231.
- Sharifzadeh M, Ansari M, Narvan M, Behnagh R A, Araee A, and Givi M K B, *T. Nonferr. Metal. SOC.* **25** (2015) 1847.
- Zhang H, Li X, Tang W, Deng X, Reynolds A P, and Sutton M A, *J. Mater. Process. Technol.* **221** (2015) 21.
- Tahmasbi K, and Mahmoodi M, *J. Manuf. Process.* **32** (2018) 151.
- Tahmasbi K, Mahmoodi M, and Tavakoli H, *T. Nonferr. Metal. SOC.* **29** (2019) 1601.
- Abu-Farha F, *Scr. Mater.* **66** (2012) 615.
- Khorrani M S, and Movahedi M, *Mater. Des.* **65** (2015) 74.
- Dinakaran I, Sathiskumar R, Vijay S J, and Murugan N, *Procedia Mater. Sci.* **5** (2014) 1502.
- Whalen S, Joshi V, Overman N, Caldwell D, Lavender C, and Skrzek T, *Magnesium Technology.* (2017) 315.
- Overman N, Whalen S, Bowden M, Olsza M, Kruska K, and Clark T, *Mater. Sci. Eng. A.* **701** (2017) 56.
- Dolatkhah A, Golbabaee P, Givi M B, and Molaiekiya F, *Mater. Des.* **37** (2012) 458.
- Ghanbari D, Asgharani M K, and Amini K, *Mechanika.* **21** (2015) 430.
- Hernández J, Medellín H, and Lange D, *Mater. Sci. Eng. A.* **650** (2016) 323.
- Baffari D, Buffa G, Campanella D, and Fratini L, *Procedia Eng.* **207** (2017) 419.
- Luo H, Shin Y, Yu Y, Cetin D, Ludwig K, and Pal U, *Appl. Surf. Sci.* **323** (2014) 65.
- Kuo L, Chen G, Chang Y S, Fu J X, Chang Y H, and Hwang W S, *Ceram. Int.* **38** (2012) 3729.
- Hiramoto M, Okinaka N, and Akiyama T, *J. Alloys Compd.* **520** (2012) 59.
- Zhang H J, Zhao L Y, and Liu X, *Trans. Indian. Inst. Met.* **73** (2020) 3019.
- Mahmoodi M, Sedighi M, and Tanner D A, *Proc. Inst. Mech. Eng., Part B: J. Eng. Manuf.* **228** (2014) 1592.
- Hafizpour H, Sanjari M, and Simchi A, *Mater. Des.* **30** (2009) 1518.
- Deore H A, Bhardwaj A, Rao A G, Mishra J, and Hiwarkar V D, *Def. Technol.* **16** (2020) 1039.
- Das H, Mondal M, Hong S T, Chun D M, and Han H N, *Int. J. Precis. Eng. Manuf.* **5** (2018) 151.
- Netto N, Zhao L, Soete J, Pyka G, and Simar A, *J. Mater. Process. Technol.* **283** (2020) 116722.
- Kumar D T A, Kumar K G B, and Pattanaik A, *Trans. Indian. Inst. Met.* **73** (2020) 3105.



- [33] Mahmoodi M, Naderi A, and Dini G, *J. Mater. Eng. Perform.* **26** (2017) 6022.
- [34] Deng X, and Chawla N, *J. Mater. Sci.* **41** (2006) 5731.
- [35] Song M, *T. Nonferr. Metal. SOC.* **19** (2009) 1400.

**Publisher's Note** Springer Nature remains neutral with regard to jurisdictional claims in published maps and institutional affiliations.